

**Along arc heterogeneity in local seismicity across
the Lesser Antilles subduction zone from a dense
ocean-bottom seismometer network**

Lidong Bie*, Andreas Rietbrock*, Stephen Hicks, Robert Allen, Jon Blundy, Valerie
Clouard, Jenny Collier, Jon Davidson, Thomas Garth, Saskia Goes, Nick Harmon, Tim
Henstock, Jeroen van Hunen, Mike Kendall, Frank Krüger, Lloyd Lynch, Colin
Macpherson, Richard Robertson, Kate Rychert, Stephen Tait, Jamie Wilkinson, Marjorie
Wilson

Corresponding author: Lidong Bie (l.bie@liv.ac.uk)

Geophysical Institute, Karlsruhe Institute of Technology, Germany

*Also at Department of Earth Ocean & Ecological Sciences, University of Liverpool, UK

ABSTRACT

The Lesser Antilles arc is only one of two subduction zones where slow-spreading Atlantic lithosphere is consumed. Slow-spreading may result in the Atlantic lithosphere being more pervasively and heterogeneously hydrated than fast-spreading Pacific lithosphere, thus affecting the flux of fluids into the deep mantle. Understanding the distribution of seismicity can help unravel the effect of fluids on geodynamic and seismogenic processes. However, a detailed view of local seismicity across the whole Lesser Antilles subduction zone is lacking. Using a temporary ocean-bottom seismic network we invert for hypocentres and 1-D velocity model. A systematic search yields a 27 km thick crust, reflecting average arc and back-arc structure. We find abundant intraslab seismicity beneath Martinique and Dominica, which may relate to the subducted Marathon/Mercurius Fracture Zones. Pervasive seismicity in the cold mantle wedge corner and thrust seismicity deep on the subducting plate interface suggest an unusually wide megathrust seismogenic zone reaching ~65 km depth. Our results provide an excellent framework for future understanding of regional seismic hazard in eastern Caribbean and the volatile cycling beneath the Lesser Antilles arc.

INTRODUCTION

Subduction zones are key centers of mass transfer in the Earth, where the lithosphere and its cargo of volatiles are recycled back into the Earth's interior. In contrast to Pacific subduction margins, where fast-spreading lithosphere is consumed, subduction of slow-spreading lithosphere such as that formed in the Atlantic should result in a more heterogeneous distribution and possibly higher amount of fluids entering the subduction zone (Escartín *et al.*, 2008). The Lesser Antilles subduction zone in Eastern Caribbean is a global end-member in that the subducting plate is relatively old (~80 Myr) but yet subducts very slowly at ~19 mm/yr (DeMets *et al.*, 2010), and it is one of two zones where the slow-spreading Atlantic oceanic lithosphere is consumed. Along-arc changes in fluid flux might affect the distribution and character of seismicity and associated volcanism. For example, pore fluids within subducting sediments may affect the seismic

character of subduction megathrusts (Heuret *et al.*, 2012), and intermediate-depth intraslab earthquakes are probably caused by dehydration embrittlement (e.g., Abers *et al.*, 2006). A coherent view of local seismicity throughout the Lesser Antilles subduction zone is thus important for understanding fluid pathways and their influence on seismicity as well as for improving seismic hazard assessment.

Available measurements for the Lesser Antilles arc indicate that subduction parameters, such as slab dip (Wadge and Shepherd, 1984), Wadati-Benioff zone thickness, and slab geometry (Bie *et al.*, 2017), vary significantly along the Lesser Antilles subduction zone. Changes in slab dip as well as thickness and depth of the Wadati-Benioff zone near 15° latitude have been attributed to either the subduction of fracture zones (Schlaphorst *et al.*, 2016; Bie *et al.*, 2017) or a slab tear and gap wide enough to allow mantle flow through (e.g., van Benthem *et al.*, 2013; Harris *et al.*, 2018; Schlaphorst *et al.*, 2017). It is debated whether these changes in slab properties mark the location of the current North-South American plate boundary (Bie *et al.* 2017) or this boundary is located further north as suggested by plate reconstructions (Bird, 2003)

There have been several studies that characterise Lesser Antilles seismicity teleseismically (e.g., McCann and Sykes, 1984; Hayes *et al.*, 2013) as well as studies of local earthquakes for some parts of the arc (e.g., Dorel *et al.*, 1981; Paulatto *et al.*, 2017; Ruiz *et al.*, 2013). These studies found higher rates of seismicity in the northern part of the Lesser Antilles subduction zone (14-18° N) than in the south, both in terms of small events and in historical records (e.g., McCann and Sykes, 1984; Hayes *et al.*, 2013). Two historic $M > 8$, presumably thrust, earthquakes have been documented in the northern Lesser Antilles (e.g., Feuillet *et al.*, 2011). However, the strength of plate interface coupling and its variation along strike remain uncertain due to sparse GPS observations and slow convergence (e.g., López *et al.*, 2006). Local studies have detected earthquakes in the fore-arc corner of the mantle wedge (Ruiz *et al.*, 2013, Laigle *et al.*, 2013), something that has only been seen in a few subduction zones worldwide (e.g., Halpaap *et al.*, 2019).

No recent efforts have systematically characterised the distribution of small-magnitude seismicity along the full extent of the Lesser Antilles plate margin. The inherent nature of oceanic subduction zones means that onshore permanent seismometer networks have limited coverage and aperture, making it difficult to accurately locate small-to-moderate magnitude earthquakes in the back- and fore-arc. Furthermore, there is no well-constrained 1-D velocity model for the Lesser Antilles, which adds to earthquake location uncertainties. As part of our Volatiles Recycling in the Lesser Antilles (VoiLA) project (Goes *et al.*, 2019), we deployed a network of 34 broadband ocean-bottom seismometers (OBS) in 2016, which were recording for 14 months. We use this OBS data, complemented by recordings from permanent and temporal land stations, to jointly invert for 1-D P- and S-wave velocity models, earthquake locations and station corrections. Our study provides the first unified reference velocity model for the Lesser Antilles region, useful for the routine location of earthquakes in the area. The recorded seismicity provides the opportunity to understand the fore- and back-arc structure, thermal structure in the mantle wedge, and deformation mechanisms at intermediate depths in the subducted slab.

SEISMIC EXPERIMENT AND DATA

In March 2016, a network of 34 broadband OBS was installed across the fore- and back-arc regions of the Lesser Antilles subduction zone (Figure 1). The OBS were retrieved in May 2017. Two stations encountered hardware failures, leaving 32 stations with useable data (Goes *et al.*, 2019). In addition to our temporal OBS observations, we collected seismic data from existing permanent stations as archived by IRIS DMC (Figure S1). We also filled the gap in permanent stations along the southern end of the arc by deploying eight temporary stations in January 2017.

Multi-channel seismic surveys were also made during expedition JC149 in April 2017. Shooting occurred along eight lines, most of which were in a north-south direction along the arc and in the back-arc, with two lines taken perpendicular to the arc in the north of the subduction zone (Figure S1). These active-source data help to constrain the shallow

velocity structure of the subduction zone, an area poorly resolved in many passive-source tomographic inversions.

MINIMUM 1-D VELOCITY MODEL

Initial Catalogue

By collating the events reported by various agencies, we created an initial earthquake catalogue for manual picking P- and S-wave onset times. Our initial catalogue includes events from the online bulletin of the International Seismological Centre (ISC), the Martinique Seismic and Volcano Observatory, and the Seismological Research Centre of the University of West Indies (hereafter, UWI-SRC). We also detected additional events using an automated short-term average ratio/long-term average (STA/LTA) triggering algorithm (Nippress *et al.*, 2010) on vertical components of the ocean-bottom stations and performed an iterative event association procedure following Rietbrock *et al.* (2012). We then manually read P- and S-wave onset times from these potential events on the ocean-bottom stations and all available onshore stations using the Seismic Data Explorer (SDX) software (<http://doree.esc.liv.ac.uk:8080/sdx>). Based on onset time uncertainties, we assigned each observation a weight as follows: Weight 0 (<0.1 s); Weight 1 (0.1–0.2 s); Weight 2 (0.2–0.5 s); Weight 3 (0.5–0.8 s); Weight 4 (>0.8 s). Initial locations were computed using the IASP91 1-D reference velocity model (Kennett and Engdahl, 1991). This workflow resulted in a total of 502 confirmed earthquakes.

We computed local magnitudes (M_L) for all events in our catalogue. Maximum amplitudes were taken from instrument-corrected waveforms, which were simulated to a Wood-Anderson seismometer. We took the largest peak-to-peak amplitude from all station components within a time window starting at the picked P-wave arrival and ending at a time window 30 seconds after the theoretical slowest travelling L_g wave (assuming a minimum L_g velocity of 3.0 km/s). We computed amplitudes for traces that had a root-mean square (RMS) signal-to-noise ratio greater than 3 to ensure that amplitude measurements were not contaminated by ocean microseism noise. We computed station magnitudes based on the M_L scale for central California (Bakun and

Joyner, 1984). Overall event magnitudes were then calculated based on a 25% trimmed-mean of station magnitudes to reject outliers. We found that station amplitudes measured at both ocean-bottom and onshore stations fit well the M_L scale over a range of hypocentral distance (see Figure S2 for examples). Regression analysis shows that our computed event local magnitudes correlate well with moment magnitude estimates for $M_w > 4.5$ events (Figure S3a), and with local duration magnitudes (M_d) for smaller events (Figure S3b).

1-D minimum velocity model inversion

Out of 502 manually picked events, we select a high-quality subset of 265 events with a maximum azimuthal gap of less than 180° , and with at least 20 P-wave and 5 S-wave arrivals. The subset consists of $\sim 10,600$ P-wave and $\sim 8,200$ S-wave arrivals for the simultaneous inversion of a 1-D layered velocity model, earthquake location and station corrections using the VELEST software (Kissling *et al.*, 1994).

The travel-time of a seismic wave is dependent on both the hypocentre parameters (origin time and location) and seismic velocity structure of the medium that the ray-path travels through. Such a coupled hypocentre-velocity problem can be solved by ray-tracing and updating the velocity model and hypocentre simultaneously (Kissling *et al.*, 1988; Eberhart-Phillips, 1990; Thurber, 1992). We conducted the simultaneous inversion using the VELEST software by Kissling *et al.* (1994). VELEST requires that all stations must be in the same velocity layer. In this study, the deepest OBS station sits ~ 5 km below sea level and the greatest land station elevation is ~ 1.4 km, making it impractical to set a model with a 7 km thick uppermost layer. Instead, we followed the strategy of Husen *et al.* (1999) and Hicks *et al.* (2014) by setting station elevations to zero and allowing station delay terms to absorb systematic travel-time errors due to elevation differences, as well as possible lateral heterogeneity in subsurface structure.

In addition to passive seismic data, we included 63 active shots from the seven shot lines (Figure 1) in order to better constrain seismic velocities at shallow depth, especially in the back-arc region, where few earthquakes with shallow hypocentral

depth occur. For each shot line, the gap between our selected neighbouring shots is roughly 15 km. The arrival times were manually picked on 22 OBS stations that record part of the 63 shots. The arrival times were corrected to subtract travel-time through the sea-water-column to be consistent with setting the station depth to sea level.

A robust initial starting velocity model is required as *a priori* information. We chose the velocity model computed by Raffaele (2011) as our starting model. Given that this model only extends to 30 km depth, we extended the starting model to a depth of 200 km by merging it with the IASP91 velocity model below 30 km depth. To search for the best-fitting minimum 1-D model, ensuring that we are not fitting local misfit minima, we perturbed the starting model randomly within ± 0.5 km/s for all layers, resulting in 1000 different synthetic starting models. The degree of convergence of the final velocity models from the 1000 inversions with different starting models is the first evidence of how robust the best-fitting model is. The velocity model that gives the minimum root-mean-square (RMS) misfit was taken as the optimal minimum 1-D velocity model.

We first invert for P-wave velocity model, using P-wave arrivals only. The best 10 velocity models with the smallest RMS misfit converge very well. We notice an increase of velocity from 7.0 to 7.7 km/s at a depth of 27 km. To test whether the Moho depth can be constrained by our datasets, we manually alter the starting model by varying the depth to the bottom of the third layer from 21 to 37 km, in 2 km increments (Figure 2a). Then the inversion is conducted in the same way as described above by generating 1000 variations of starting models for each Moho depth scenario and searching for the best model that gives minimum RMS. We then plotted the minimum RMS values versus the prescribed Moho depths, and the comparison shows a preferred average Moho depth of 27 km (Figure 2c).

After obtaining the best P-wave velocity model and optimal Moho depth, we subsequently inverted for S-wave velocity model using P- and S-wave arrival times. Similarly, 1000 variations of S-wave starting velocity model are generated, based on the P-wave velocity model and average v_p/v_s ratio derived from Wadati analysis. Due to the

trade-off between station corrections and the top layer velocity, we chose not to fix the top layer P-wave velocity as derived from the inversion.

Characteristics of Minimum 1-D Velocity Model

Tests with a range of starting models with various Moho depth (Figure 2a) result in the final minimum 1-D velocity model shown in Figure 2b. The best-fitting 1-D minimum velocity model comprises two layers of upper-plate crust underlying a top sedimentary layer. The estimated crustal P-wave velocity increases from 4.3 km/s at shallow depth to 7.7 km/s at 27 km depth. Affected by mostly near-vertical ray-paths, the uppermost crustal layer velocity is less well constrained, shown by poor convergence of the 10 best models, implying strong spatial variation of uppermost crustal velocity. This does not influence the final earthquake locations however, as our analysis of locations corresponding to the best 10 velocity models show a small average shift of <100 meters in all directions. The average velocities for the two main crustal layers are 6.3 km/s and 7.0 km/s, consistent with those determined by Boynton *et al.* (1979) for the island arc. Our systematic search with varying crustal thickness yields a minimum misfit when the Moho depth is 27 km (Figure 2c). Crustal thicknesses derived by González *et al.* (2018) from surface wave and receiver function analysis under 19 land stations along the arc vary from 21 km beneath St Lucia to 33 km beneath Grenada in the south, with an average of 26 km (Figure 2c), which is similar to our model value even though this constitutes an average across the margin. Between 27 km and 200 km depth, the P-wave velocity (v_p) and S-wave velocity (v_s) increasing steadily to 8.7 km/s and 4.9 km/s, respectively, fits the observations (Table S1).

Station corrections are incorporated to compensate 3-D heterogeneity of near-surface velocity and station elevations. Station corrections for v_p are generally smaller than 0.5 s, while for v_s , the station corrections are larger but mostly below 1.0 s (Figure 3). There are some systematic patterns, including positive corrections (i.e., thicker or slower crust) north and negative corrections south of reference station DP05 near Martinique in the central arc, as well as a linear correlation between station elevation and correction for

the OBS (Figure S4). Based on active source imaging (Allen *et al.*, 2019), our preferred interpretation is a systematic variation in crustal thickness from north to south.

OVERALL CHARACTERISTICS OF LA SEISMICITY AND SUBDUCTION GEOMETRY

The best-fitting velocity model is used to relocate the original 502 manually-picked events. We conducted hypocentre location stability tests by randomly perturbing hypocentres ± 7.5 -12.5 km in 3-D, then relocating using the best-fitting 1-D velocity model (Figure 2b). When the azimuthal gap is less than $\sim 270^\circ$, the earthquakes generally relocate back to their original positions (Figure 4a), with a standard deviation of 0.21, 0.17, and 0.77 km for latitude, longitude and depth, respectively (Figure 4b). In addition to the azimuthal gap, we retained events that were relocated within 5 km depth variation from the original position. Strict filtering after hypocentre location stability tests resulted in 378 well-relocated events (Figure 5).

Although our observation period is short, the relocated seismicity exhibits a higher rate in the northern part of the subduction zone than in the south (Figure 5 and 6), consistent with previous studies (e.g., Bie *et al.*, 2017). Sparse seismicity is observed in the forearc region within 50 km distance from the trench. However, station coverage close to the trench in the outer forearc is very limited, so detection and location accuracy here is reduced. Most seismicity beneath the outer forearc is found in the north, where the forearc is less wide, and OBS stations were closer to the trench. We note that more smaller earthquakes may be found using template-matching techniques (e.g., Zhu *et al.*, 2019). Here, we focussed on the larger events with robust arrival time determination, particularly for the generation of a well-constrained 1-D seismic velocity, with less emphasis on the evolution of seismicity in time and space.

Seismicity extends from the shallow upper crust of the overriding plate to intermediate depths of 180 km in the central slab (Figure 5). The distribution of seismicity with depth displays two peaks (see inset to Figure 5). Shallow seismicity increases with depth and

reaches its first peak at ~25 km, stays relatively high until there is a sharp reduction below ~60 km depth. At depths greater than ~80 km, seismicity increases again to depth of 170 km. The shallow peak comprises events in the overlying arc crust, and between about 25 and 60 km depth, events along the plate interface and in the mantle wedge corner. The deep peak consists of events within the subducting slab. The depth ranges of these peaks are similar to those that Paulatto *et al.* (2017) identified below Martinique, who proposed that the peaks in mantle wedge and slab seismicity are associated with slab dehydration around 40 and 150 km depth. In Section 5 we discuss the seismicity in each part of the system in detail.

Our catalogue of regional seismicity provides new constraints on slab geometry. As shown in Figure 5, the seismicity distribution in this study does not agree well with the global Slab2 plate geometry model (Hayes *et al.*, 2018). The slab surface in Slab2 is up to 70 km shallower at depth of 180 km. Our seismicity is consistent with the teleseismically-constrained slab geometry of Bie *et al.* (2017) to ~80 km depth, while beyond that, seismicity in our study suggests a slightly steeper slab (profiles B-B', C-C', and D-D' in Figure S5). We thus integrated the local seismicity in this study with the global datasets used in Bie *et al.* (2017) and constructed a refined slab geometry (Figure 5). How the large difference in slab geometry affects geodynamic modelling and seismic hazard estimation will be a subject of a planned future study.

DISCUSSION

Earthquakes in the Overriding Plate

The shallow events lie in the overriding upper plate, reflecting fault failures in the fore-arc and/or are related to volcanic structures along the arc. Profile A-A' shows a cluster of events ~100 km westward of the trench at 14-25 km depth. These events are mostly aftershocks of the M_w 5.7 thrust earthquake on 17 April 2017. The trenchward-dipping alignment of the cluster may indicate failure of a back-thrust fault bounding the western edge of the accretionary prism. A similar cluster can be found ~150 km west of the trench in profile B-B'. It is unclear whether this cluster on B-B' was on splay thrusts or

back-thrusts, given no clear alignment is shown and the relatively large RMS misfit values.

Profile B-B' shows another cluster of shallow seismicity in line with the volcanic arc, between Guadeloupe and Dominica. This seismicity can be divided into two sequences. The first in 2016 starts with M_L 4.5 and M_L 4.1 events on 12 April, and lacks a clear subsequent aftershock sequence. The second sequence swarm started in April 2017 denoted by a M_L 3.5 earthquake (Table S2). Previously on 21 November 2004, this area experienced a M_w 6.3 normal fault earthquake on the Roseau fault, which bounds the western side of the Les Saintes Graben between Guadeloupe and Dominica (Bazin *et al.*, 2010). The mainshock was followed by a long-lasting aftershock sequence on the Roseau Fault and a short-lived aftershock sequence on the smaller antithetic normal faults. Bazin *et al.* (2010) attributed the long-lasting aftershock sequence on the Roseau fault to this region being strongly faulted and filled with fluids, as inferred from a low v_p anomaly and a high v_p/v_s ratio, while for the short duration aftershock sequence, fluid was less involved. This interpretation of high fluid content is consistent with our observation of occasional swarm activity in this region.

Below Tobago, in the southern fore-arc, a sequence of aftershocks followed the M_w 5.9 strike-slip earthquake on 6 December 2016 (profile E-E' of Figure 5). Although, we expected these to be upper plate events, the aftershocks were relocated to ~60 km depth. A M_w 6.1 earthquake with a similar faulting mechanism occurred on 2 April 1997 at 45 km depth (NEIC), preceding a larger M_w 6.7 normal fault earthquake on 22 April 1997 at a much shallower depth of 5-15 km (NEIC). The GCMT focal mechanism for the 2016 event suggests either sinistral strike-slip on an E-W striking sub-vertical (dip 67°) fault plane, or dextral strike-slip rupture on a near-vertical (80° dip) N-S striking fault (Figure 6). This mechanism is not consistent with the current active E-W dextral shearing across the Caribbean-South American plate boundary zone (e.g., Weber *et al.*, 2015). These strike-slip events lie anomalously deep beneath the fore-arc, and the 2016 cluster is close to the top of the subducting slab (profile E-E' of Figure 5). A likely

explanation is that the 2016 and 1997 strike-slip events ruptured structures within the down-going oceanic crust.

Mantle Wedge Seismicity

In addition to shallow upper crust activity, seismicity in the overriding plate appears in the mantle wedge corner above ~65 km depth and reaches into the lower crust (profiles in Figure 5), consistent with Ruiz *et al.* (2013) and Laigle *et al.* (2013). Seismicity in the mantle-wedge corner has implications for the thermal structure of the mantle wedge. It is normally assumed that the stable-unstable sliding transition in oceanic mantle occurs at temperatures of ~600°C (e.g., McKenzie *et al.*, 2005). By constructing an approximate curve delineating the wedge-shaped mantle corner seismicity, we found that the inferred transition consistently intersects the slab (red curve constrained by seismicity in Figure 5 profiles) at ~65 km depth across the subduction zone. In contrast to profiles in the north, the lack of mantle wedge seismicity in the EE' profile suggests that the mantle wedge temperature is different from north to south.

Mantle-wedge corner seismicity has been reported in only a few subduction zones around the world besides the Antilles, namely, NE Japan, New Zealand, Columbia and Greece. Such events have been attributed to the deformation of subducted seamounts (Uchida *et al.*, 2010), or hydraulic fracturing/fluid-assisted embrittlement or weakening due to the ascent of fluids from the slab (Chang *et al.*, 2017, Halpaap *et al.*, 2019). If this is the case for the Lesser Antilles, then the mantle wedge earthquakes may represent an unusual pathway for fluids driven off by early metamorphic reactions in the subducting plate. Alternatively, in a mantle wedge of mixed chemical composition (Laigle *et al.*, 2013), preferential hydration of the peridotite components may result in a differential volume change that may open fractures, causing extensional faulting in the mantle wedge (Iyer *et al.*, 2008).

Plate Interface Seismicity

In the north, interplate seismicity is observed from depths of about 10 km, while in the south, the shallowest seismicity is at 30 km depth at 14°N, and 45 km south of 12°N

(profiles in Figure 5). The largest thrust earthquake (M_w 5.8) on the plate interface during our deployment occurred on 3 February 2017 east of Martinique. The Martinique earthquake was followed by aftershocks at ~ 50 km depth (profile C-C'). We relocated the M_w 5.8 mainshock to 51 km depth. The alignment of the sequence with the slab geometry indicates rupture of the plate interface and suggests a seismogenic zone reaching to at least 60 km depth, deeper than the fault locking depth of 5-25 km previously proposed by Symithe *et al.* (2015) using geodetic observations.

The Martinique sequence occurred deeper than the intersection of the upper plate Moho (~ 27 km) with the down-going plate interface. This observation is similar to that found by Ruiz *et al.* (2013) of seismic activity offshore Martinique and Dominica, suggesting that the interplate seismogenic zone width is usually not limited by thickness of the upper plate crust, consistent with a global compilation by Heuret *et al.* (2011). However, the down-dip limit of ~ 65 km depth that we find for the Lesser Antilles megathrust seismogenic zone is high compared to the global range of 51 ± 8 km (Heuret *et al.*, 2011). The Martinique sequence on the plate interface, together with supra-slab seismicity discussed in the previous section, suggest the existence of a cold mantle nose, which can effectively extend the decoupling depth of the slab and upper plate mantle (Wada and Wang, 2009). This wide seismogenic zone has important implications for the maximum magnitude of earthquakes that could occur in this region, and this may explain the large magnitudes of the Guadeloupe earthquakes in the 1800s. An alternative to this is that this deeper part may represent seismic-aseismic transitional zone (e.g., Lay et al., 2012). Although large earthquakes may not initiate at this deeper depth, rupture may propagate into this region and effectively increase the earthquake magnitude and thus seismic hazard.

Intermediate Depth Seismicity

The Lesser Antilles Wadati-Benioff zone extends to 150-180 km depth with a concentration of intraslab seismicity beneath the center of the arc, between the islands of Guadeloupe and St. Lucia (Figure 5). During our experiment, a M_w 5.6 earthquake occurred on 18 October 2016 southwest of Dominica at ~ 160 km depth. This event had

a normal faulting mechanism with both nodal planes striking perpendicular to the arc, and in the direction of convergence. Normal faulting earthquakes are frequent within the slab at ~150 km depth between the islands of Dominica and Martinique, i.e. in the region with the densest intermediate depth seismicity. Similar recent moderate-to-large intraplate events (Figure 6) include a M_w 5.6 on 28 December 2015, a M_w 7.4 on 29 November 2007, and a M_w 5.8 on 24 September 1996 and an earlier magnitude 7.5 that occurred on 19 March 1953 (Stein *et al.*, 1983) ~100 km south of the 2016 event. According to the GCMT earthquake catalogue, all those events since the 1990s share a similar, normal faulting mechanism with a minor strike-slip component; at least one of the nodal planes strikes parallel with the subduction direction.

Fault strikes parallel or oblique to the trench could be due to reactivation of subducted outer-rise normal faults formed at the mid-oceanic spreading ridge (e.g., Delouis and Legrand, 2007; Garth and Rietbrock, 2014). However, trench-perpendicular nodal plane ruptures cannot be explained in this manner. Instead, the intermediate-depth normal fault earthquakes mentioned above occurred around the projected positions of the subducted Marathon and Mercurius Fracture zones (Figure 6). This finding may suggest a link between the deep normal fault earthquakes and subducted fracture zones – which may be effective vessels to bring water to intermediate depths. Thus, the reactivation of inherited oceanic structures (e.g., fractures zones), facilitated by dehydration embrittlement, may be the dominant mechanism responsible for the normal faulting events seen at intermediate depth in the central arc. In other places along the arc, intermediate depth normal fault earthquakes are rare, which may suggest weaker hydration and smaller fluid fluxes, insufficient to drive significant dehydration embrittlement failure.

Slab Tear?

The coherent catalogue of seismicity compiled for this study offers a chance to test the hypothesis that a slab tear exists at 15°N - between the islands of Dominica and Martinique – as suggested by teleseismic tomography models and seismic anisotropy observations (Van Benthem *et al.*, 2013; Harris *et al.*, 2018; Schlaphorst *et al.*, 2017).

We projected seismicity in this area onto multiple profiles (with a 10 km gap between neighbouring profiles) perpendicular to the trench and marked those to the north of the profile in blue, and those to the south in red (Figure S6). This method can reveal the location of a slab tear, if two seismicity alignments with different dip angles are observed. Our results do not indicate any distinctive change in dip angle but rather a thickening of the Wadati-Benioff zone from north to south as shown by line 7 in Figure S6. The thickening here may define the northern boundary of the subducted Marathon Fracture zone. Seismicity during the period of our observation does not support the notion that a large-scale slab tear exists at this depth, but we cannot rule out a slab tear below the deepest seismicity.

CONCLUSIONS

In this study, we used seismic data from a dense OBS network to record local seismicity in the Lesser Antilles subduction zone and delineate changes in seismic deformation and velocity structure both with depth and along the arc. The joint inversion for a 1-D velocity model, earthquake location and station corrections yields an optimal crustal thickness of 27 km, representative of an arc-back-arc average. Abundant intermediate-depth seismicity is found beneath the islands of Martinique and Dominica, which may relate to the subducted Marathon and Mercurius Fracture Zones. Although a slab tear near 15°N has been proposed by previous teleseismic seismic studies, our seismicity distribution suggests thickening of the Wadat-Benioff zone, but without distinctive changes in the slab dip angle that would be expected for a tear. Interpretations of our earthquake locations reveal pervasive seismicity in the cold mantle wedge corner, which is not observed in many subduction zones. Together with the deep 2016 Martinique earthquake sequence on the plate interface, these observations suggest an abnormally cold and, therefore, wide megathrust seismogenic zone reaching ~65 km depth. It is worth to further investigate whether these features are inherent to the slow subduction of slow-spreading oceanic lithosphere in the Atlantic. These results provide a new framework for advances in operational earthquake locations and future estimation of seismic hazard in the Eastern Caribbean.

DATA AND RESOURCES

The optimal 1-D velocity model is made available in the electronic supplement to this article (Table S1). The relocated earthquake catalogue is available in Table S2. The Global Centroid Moment Tensor Project database was searched using www.globalcmt.org/CMTsearch.html (last accessed on April 1, 2019). We made figures using GMT (Wessel and Smalley, 1998). Supplemental content for this article includes figures showing the quality of earthquake magnitude estimation, the relationship between station correction and elevation, the comparison of our slab geometry with that of Slab2.0, and seismicity projected to dense profiles in the central part of the arc.

ACKNOWLEDGEMENTS

This work was funded under NERC grant NE/K010611/1. We thank the “German Instrument Pool for Amphibian Seismology (DEPAS)”, hosted by the Alfred Wegener Institute Bremerhaven, for providing the ocean-bottom seismometers and temporary island seismometers, and UCSD (Scripps) for providing additional ocean-bottom seismometers. We thank Allison Bent, Zhigang Peng, Hongfeng Yang, and two anonymous reviewers for their helpful and constructive comments.

REFERENCES

- Allen, R., J. Collier, T. Henstock, A. Stewart, and S. Goes, 2019, A new tectonic model for the Lesser Antilles: Evidence for a buried arc in the eastern Caribbean, *Geophysical Research Abstract*, 21, EGU2019-7944
- Bakun, W. H., and W. B., Joyner (1984), The ML scale in central California, *Bull. Seismol. Soc. Am.*, 74(5), 1827-1843.
- Bie, L., T. Garth, and A. Rietbrock, 2017, Links between the distribution of intermediate depth seismicity and structure of the incoming plate in the Lesser Antilles arc, In AGU Fall Meeting Abstracts. #T31D-0672
- Abers, G. A., P. E. van Keken, E. A. Kneller, A. Ferris, and J. C. Stachnik (2006), The thermal structure of subduction zones constrained by seismic imaging: Implications for slab dehydration and wedge flow, *Earth Planet. Sci. Lett.*, 241(3-4), 387-397.
- Bazin, S., N. Feuillet, C. Duclos, W. Crawford, A. Nercissian, M. Bengoubou-Valérius, et al., (2010), The 2004–2005 Les Saintes (French West Indies) seismic aftershock sequence observed with ocean bottom seismometers, *Tectonophysics*, 489(1-4), 91-103.
- Bird, P. (2003), An updated digital model of plate boundaries, *Geochem. Geophys. Geosyst.*, 4(3), 1027, doi:10.1029/2001GC000252.
- Boynton, C. H., G. K. Westbrook, M. H. P. Bott, and R. E. Long (1979), A seismic refraction investigation of crustal structure beneath the Lesser Antilles island arc, *Geophys. J. R. Astron. Soc.*, 58, 371–393.
- Chang, Y., L. M. Warren, and G. A. Prieto (2017), Precise Locations for Intermediate-Depth Earthquakes in the Cauca Cluster, Colombia, *Bull. Seismol. Soc. Am.*, 107(6), 2649-2663.
- Delouis, B., and D. Legrand (2007), Mw 7.8 Tarapaca intermediate depth earthquake of 13 June 2005 (northern Chile): Fault plane identification and slip distribution by waveform inversion, *Geophys. Res. Lett.*, 34(1).
- DeMets, C., R. G. Gordon, and D. F. Argus (2010), Geologically current plate motions, *Geophys. J. Int.*, 181, 1–80.
- Dorel, J. (1981), Seismicity and seismic gap in the Lesser Antilles arc and earthquake hazard in Guadeloupe, *Geophys. J. R. Astron. Soc.*, 67(3), 679-695.
- Eberhart-Phillips, D. (1990), Three-dimensional P and S velocity structure in the Coalinga region, California. *J. Geophys. Res.*, 95(B10), 15343-15363.

- Escartín, J., D. K. Smith, J. Cann, H. Schouten, C. H. Langmuir, and S. Escrig (2008), Central role of detachment faults in accretion of slow-spreading oceanic lithosphere, *Nature*, 455(7214), 790.
- Feuillet, N., F. Beauducel, and P. Tapponnier (2011), Tectonic context of moderate to large historical earthquakes in the Lesser Antilles and mechanical coupling with volcanoes, *J. Geophys. Res.*, 116(B10), doi:10.1029/2011JB008443
- Garth, T., and A. Rietbrock (2014), Downdip velocity changes in subducted oceanic crust beneath Northern Japan-insights from guided waves, *Geophys. J. Int.*, 198(3), 1342-1358. doi:10.1093/gji/ggu206
- González, O., V. Clouard, and J. Zahradnik (2017), Moment tensor solutions along the central Lesser Antilles using regional broadband stations, *Tectonophysics*, 717, 214-225.
- González, O., V. Clouard, S. Tait, and G. F. Panza (2018), S-wave velocities of the lithosphere-asthenosphere system in the Lesser Antilles from the joint inversion of surface wave dispersion and receiver function analysis, *Tectonophysics*, 734, 1-15.
- Halpaap, F., S. Rondenay, A. Perrin, S. Goes, L. Ottemöller, H. Austrheim, R. Shaw, and T. Eeken (2019), Earthquakes track subduction fluids from slab source to mantle wedge sink, *Sci. Adv.*, 5(4), DOI: 10.1126/sciadv.aav7369.
- Harris, C. W., M. S. Miller, and R. W. Porritt (2018), Tomographic Imaging of Slab Segmentation and Deformation in the Greater Antilles, *Geochem. Geophys. Geosyst.*,
- Hayes, G. P., D. E. McNamara, L. Seidman, and J. Roger (2013), Quantifying potential earthquake and tsunami hazard in the Lesser Antilles subduction zone of the Caribbean region, *Geophys. J. Int.*, 196(1), 510-521.
- Hayes, G. P., G. L. Moore, D. E. Portner, M. Hearne, H. Flamme, M. Furtney, and G. M. Smoczyk (2018), Slab2, a comprehensive subduction zone geometry model, *Science*, 362(6410), 58-61.
- Heuret, A., C. P. Conrad, F. Funiciello, S. Lallemand, and L. Sandri (2012), Relation between subduction megathrust earthquakes, trench sediment thickness and upper plate strain, *Geophys. Res. Lett.*, 39(5).
- Heuret, A., S. Lallemand, F. Funiciello, C. Piromallo, and C. Faccenna (2011), Physical characteristics of subduction interface type seismogenic zones revisited, *Geochem. Geophys. Geosyst.*, 12(1).
- Hicks, S., A. Rietbrock, I. Ryder, C. Lee, and M. Miller (2004), Anatomy of a megathrust: The 2010 M8.8 Maule, Chile earthquake rupture zone imaged using seismic tomography, *Earth Planet. Sci. Lett.*, 405, 142-155, doi.org/10.1016/j.epsl.2014.08.028

- 561
- 562 Husen, S., E. Kissling, E. Flueh, and G. Asch (1999), Accurate hypocentre
- 563 determination in the seismogenic zone of the subducting Nazca Plate in northern Chile
- 564 using a combined on/offshore network, *Geophys. J. Int.*, 138(3), 687-701.
- 565
- 566 Iyer, K., B. Jamtveit, J. Mathiesen, A. Malthé-Sørenssen, and J. Feder (2008),
- 567 Reaction-assisted hierarchical fracturing during serpentinization, *Earth Planet. Sci. Lett.*,
- 568 267(3-4), 503-516.
- 569
- 570 Kennett B. L. N., and E. R. Engdahl (1991), Travel times for global earthquake location
- 571 and phase association, *Geophys. J. Int.*, 105, 429-465.
- 572
- 573 Kissling, E., W. L. Ellsworth, D. Eberhart-Phillips, and U. Kradolfer (1994), Initial
- 574 reference models in local earthquake tomography, *J. Geophys. Res.*, 99, 19,635–
- 575 19,646, doi:10.1029/93JB03138.
- 576
- 577 Kissling, E. (1988), Geotomography with local earthquake data, *Rev. Geophys.*, 26(4),
- 578 659-698.
- 579
- 580 Laigle, M., A. Hirn, M. Sapin, A. Bécel, P. Charvis, E. Flueh, et al., (2013), Seismic
- 581 structure and activity of the north-central Lesser Antilles subduction zone from an
- 582 integrated approach: Similarities with the Tohoku forearc, *Tectonophysics*, 603, 1-20.
- 583
- 584 Lay, T., H. Kanamori, C. J. Ammon, K. D. Koper, A. R. Hutko, L. Ye, H. Yue, and T. M.
- 585 Rushing (2012), Depth-varying rupture properties of subduction zone megathrust
- 586 faults. *J. Geophys. Res.*, 117(B4311), doi:10.1029/2011JB009133.
- 587
- 588 López, A. M., S. Stein, T. Dixon, G. Sella, E. Calais, P. Jansma, Weber, and P.
- 589 LaFemina (2006), Is there a northern Lesser Antilles forearc block?, *Geophys. Res.*
- 590 *Lett.*, 33(7).
- 591
- 592 McCann, W. R., and L. R. Sykes (1984), Subduction of aseismic ridges beneath the
- 593 Caribbean plate: Implications for the tectonics and seismic potential of the northeastern
- 594 Caribbean, *J. Geophys. Res.*, 89(B6), 4493-4519.
- 595
- 596 McKenzie, D., J. Jackson, and K. Priestley (2005), Thermal structure of oceanic and
- 597 continental lithosphere, *Earth Planet. Sci. Lett.*, 233(3-4), 337-349.
- 598
- 599 Nippres, S. E. J., A. Rietbrock, and A. E. Heath (2010), Optimized automatic pickers:
- 600 application to the ANCORP data set. *Geophys. J. Int.*, 181(2), 911-925.
- 601
- 602 Paulatto, M., M. Laigle, A. Galve, P. Charvis, M. Sapin, G. Bayrakci, ... and H. Kopp
- 603 (2017), Dehydration of subducting slow-spread oceanic lithosphere in the Lesser
- 604 Antilles, *Nat. Comm.*, 8, 15980.
- 605

- Raffaele, R. M. (2011), Seismic structure of subduction zone of the Lesser Antilles, PhD thesis, University of Catania.
- Rietbrock, A., I. Ryder, G. Hayes, C. Haberland, D. Comte, S. Roecker, and H. Lyon-Caen (2012), Aftershock seismicity of the 2010 Maule Mw8.8, Chile, earthquake: Correlation between co-seismic slip models and aftershock distribution? *Geophys. Res. Lett.*, 39(8). doi:10.1029/2012GL051308.
- Ruiz, M., A. Galve, T. Monfret, M. Sapin, P. Charvis, M. Laigle, ... and J. Diaz (2013), Seismic activity offshore Martinique and Dominica islands (Central Lesser Antilles subduction zone) from temporary onshore and offshore seismic networks, *Tectonophysics*, 603, 68-78.
- Goes, S., et al. (2019), Project VoiLA: Volatile Recycling in the Lesser Antilles, *Eos*, 100, <https://doi.org/10.1029/2019EO117309>.
- Schlaphorst, D., J. M. Kendall, J. S. Collier, J. P. Verdon, J. Blundy, B. Baptie, ... and M. P. Bouin (2016), Water, oceanic fracture zones and the lubrication of subducting plate boundaries—insights from seismicity, *Geophys. J. Int.*, 204(3), 1405-1420.
- Schlaphorst, D., J. M. Kendall, B. Baptie, J. L. Latchman, and S. Tait (2017), Gaps, tears and seismic anisotropy around the subducting slabs of the Antilles, *Tectonophysics*, 698, 65-78.
- Stein, S., J. F. Engeln, D. A. Wiens, R. C. Speed, and K. Fujita (1983), Slow subduction of old lithosphere in the Lesser Antilles, *Tectonophysics*, 99(2-4), 139-148.
- Symithe, S., E. Calais, J. B. De Chabaliere, R. Robertson, and M. Higgins (2015), Current block motions and strain accumulation on active faults in the Caribbean, *J. Geophys. Res.*, 120(5), 3748-3774.
- Thurber, C. H. (1992), Hypocenter-velocity structure coupling in local earthquake tomography, *Phys. Earth Planet. In.*, 75(1-3), 55-62.
- Uchida, N., S. H. Kirby, T. Okada, R. Hino, and A. Hasegawa (2010), Supraslab earthquake clusters above the subduction plate boundary offshore Sanriku, northeastern Japan: Seismogenesis in a graveyard of detached seamounts?, *J. Geophys. Res.*, 115(B9).
- van Benthem, S., R. Govers, W. Spakman, and R. Wortel (2013), Tectonic evolution and mantle structure of the Caribbean, *J. Geophys. Res.*, 118(6), 3019-3036.
- Wada, I., and K. Wang (2009), Common depth of slab-mantle decoupling: Reconciling diversity and uniformity of subduction zones, *Geochem. Geophys. Geosyst.*, 10(10).

Wadge, G., and J. B. Shepherd (1984). Segmentation of the Lesser Antilles subduction zone, *Earth Planet. Sci. Lett.*, 71(2), 297-304.

Weber, J. C., H. Geirsson, J. L. Latchman, K. Shaw, P. La Femina, S. Wdowinski, et al., (2015), Tectonic inversion in the Caribbean-South American plate boundary: GPS geodesy, seismology, and tectonics of the Mw 6.7 22 April 1997 Tobago earthquake, *Tectonics*, 34(6), 1181-1194.

Wessel, P., and R. Smalley (1998). New, improved version of generic mapping tools released, *Eos Trans. AGU* 79, no. 47, 579-579.

Zhu, G., H. Yang, J. Lin, Z. Zhou, M. Xu, J. Sun, and K. Wan (2019), Along-strike variation in slab geometry at the southern Mariana subduction zone revealed by seismicity through ocean bottom seismic experiments, *Geophys. J. Int.*, 218(3), 2122-2135, doi:10.1093/gji/ggz272.

666 *Lidong Bie*
667 *Andreas Rietbrock*
668 *Geophysical Institute, Karlsruhe Institute of Technology, Germany*
669 *Department of Earth Ocean & Ecological Sciences, University of Liverpool, UK*
670 l.bie@liv.ac.uk
671
672 *Stephen Hicks*
673 *Robert Allen*
674 *Jenny Collier*
675 *Saskia Goes*
676 *Department of Earth Science & Engineering, Imperial College London, UK*
677
678 *Jon Blundy*
679 *Mike Kendall*
680 *School of Earth Sciences, University of Bristol, UK*
681
682 *Nick Harmon*
683 *Tim Henstock*
684 *Kate Rychert*
685 *Department of Ocean & Earth Sciences, University of Southampton, UK*
686
687 *Jon Davidson(Deceased)*
688 *Colin Macpherson*
689 *Jeroen van Hunen*
690 *Department of Earth Sciences, University of Durham, UK*
691
692 *Valerie Clouard*
693 *Stephen Tait*
694 *Institut de Physique du Globe de Paris, Université Paris Diderot, France*
695
696 *Thomas Garth*

697 *Department of Earth Sciences, University of Oxford, UK*

698

699 *Lloyd Lynch*

700 *Richard Robertson*

701 *Seismic Research Centre, The University of the West Indies, Trinidad and Tobago*

702

703 *Frank Krüger*

704 *Institute of Geosciences, University of Potsdam, Germany*

705

706 *Jamie Wilkinson*

707 *Natural History Museum, London, UK*

708

709 *Marjorie Wilson*

710 *School of Earth & Environment, University of Leeds*

711

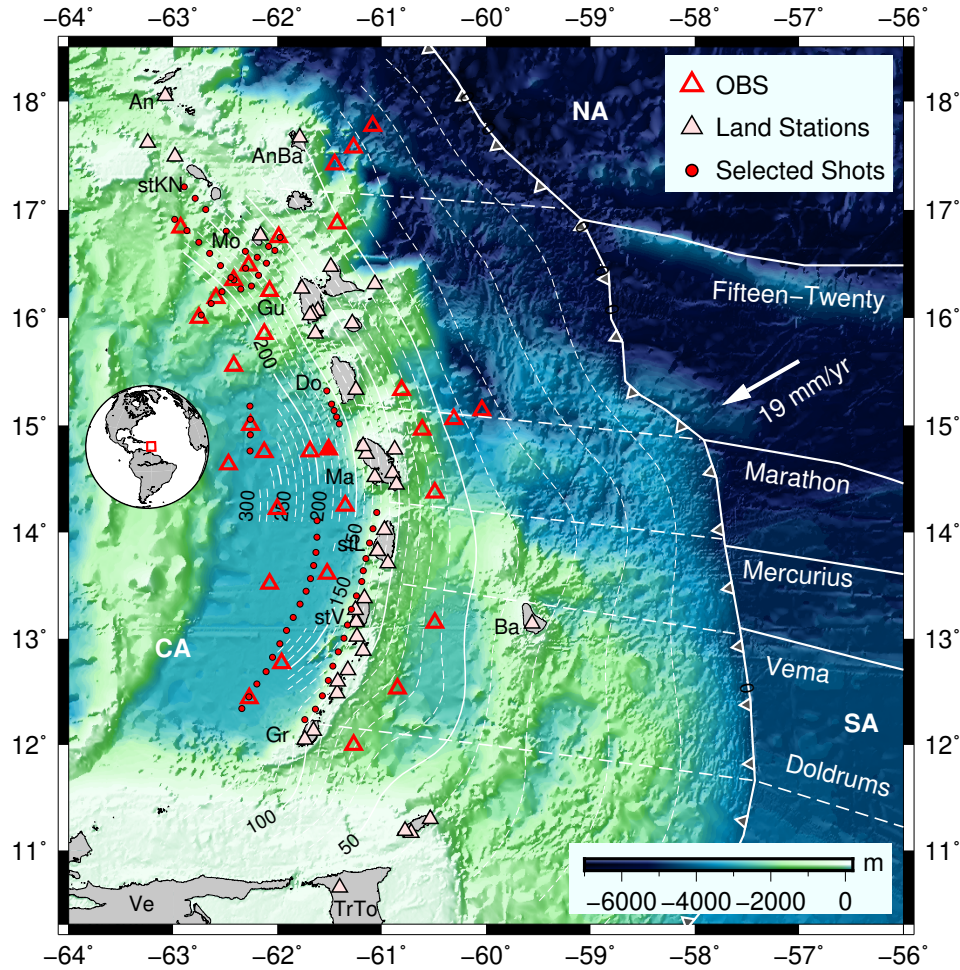


Figure 1. Tectonic map of the Lesser Antilles subduction zone. Offshore and onshore seismic stations used in this study are marked by empty red and filled triangles, respectively. Light white contours depict refined slab geometry from this study. Reference station in the 1-D velocity inversion is filled by red colour. Red dots in the back-arc indicate active shots included in the inversion. Details of land stations incorporated in this study are shown in Figure S1. Inferred fracture zone and spreading-ridge structures (Schlaphorst *et al.*, 2016) are shown with white lines. CA: Caribbean Plate; NA: North American Plate; SA: South American Plate. See Figure S1 for details of island name abbreviations.

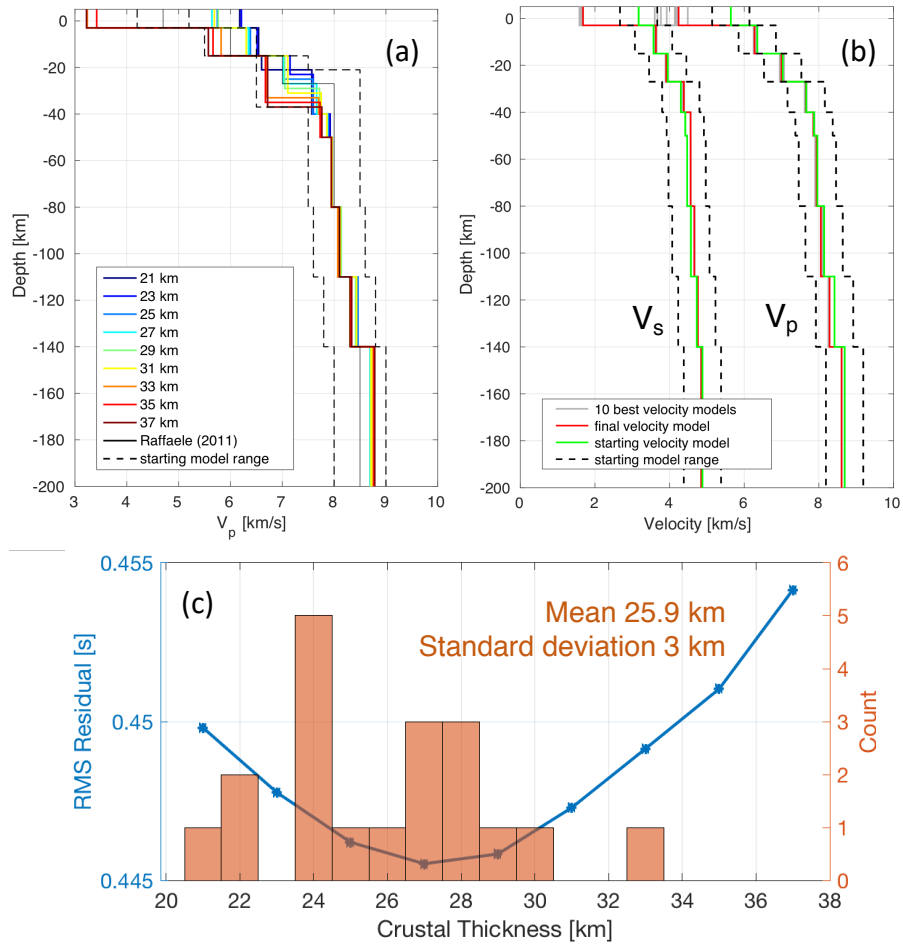


Figure 2. (a) Best v_p models for simulations with different starting velocity layer configuration. The crustal thickness is varied from 21 km to 37 km, in 2 km increments. (b) Final v_p and v_s models for the Lesser Antilles subduction zone. (c) RMS residual versus the tested crustal thickness. The minimum RMS misfit is achieved with a crustal thickness of 27 km. The bar chart shows the distribution of crustal thickness derived by González et al. (2018) from 19 land stations along the arc.

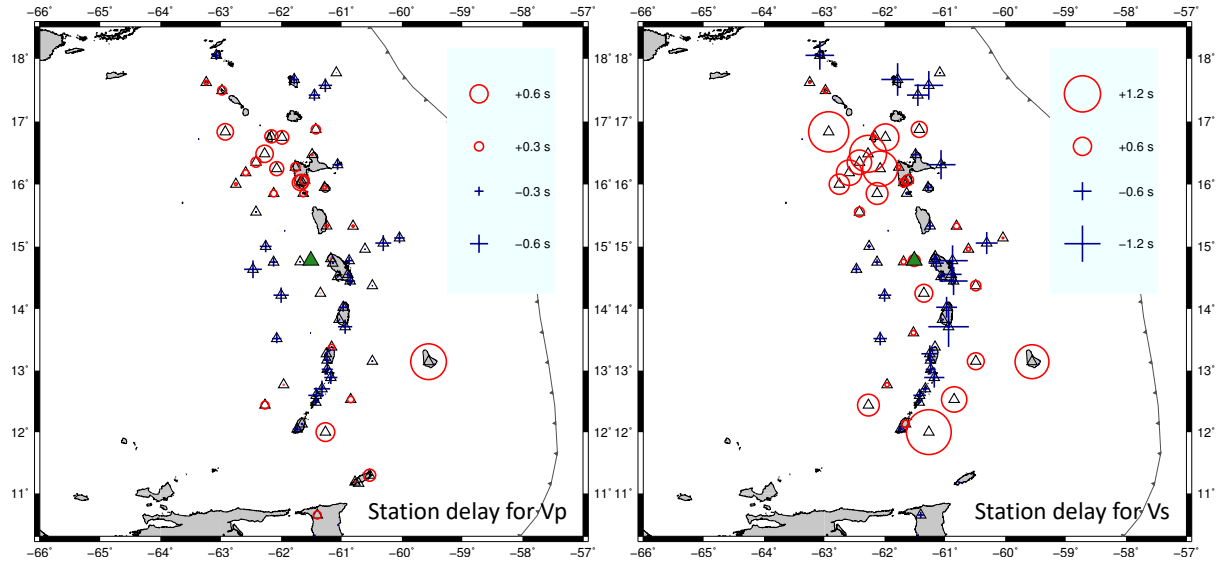


Figure 3. Station corrections associated with the velocity model shown in Figure 2b.

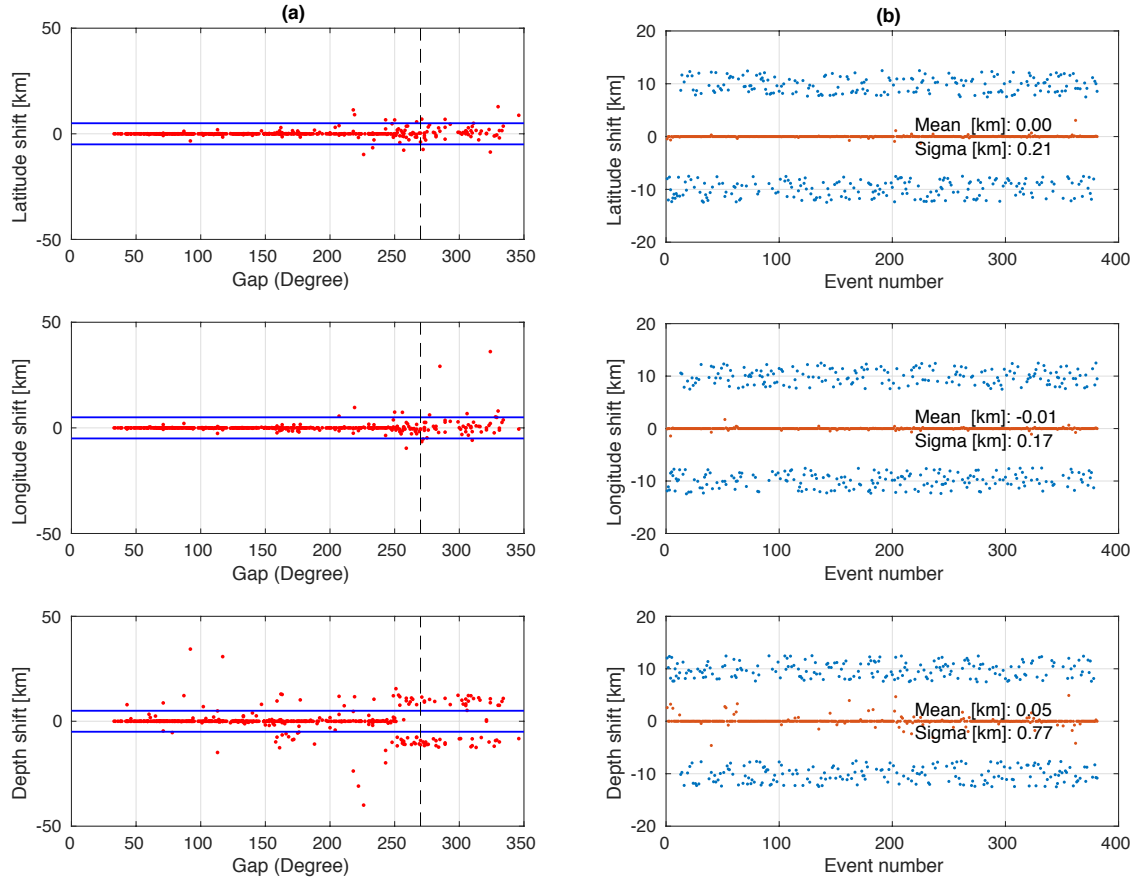


Figure 4. Stability test using the velocity model shown in Figure 2b to recover the randomly perturbed earthquakes (blue points) in the longitude, latitude and depth directions. Those recovered (red points) to be within 5 km (marked as blue line in the left panels) from their original locations and having azimuthal gap smaller than 270° (black dashed line) are deemed as events with good quality and shown in Figure 5 and 6. The panels on the right side show the mean and standard deviation of the difference between the recovered (red points) and perturbed (blue points) earthquake locations in three directions for good quality events.

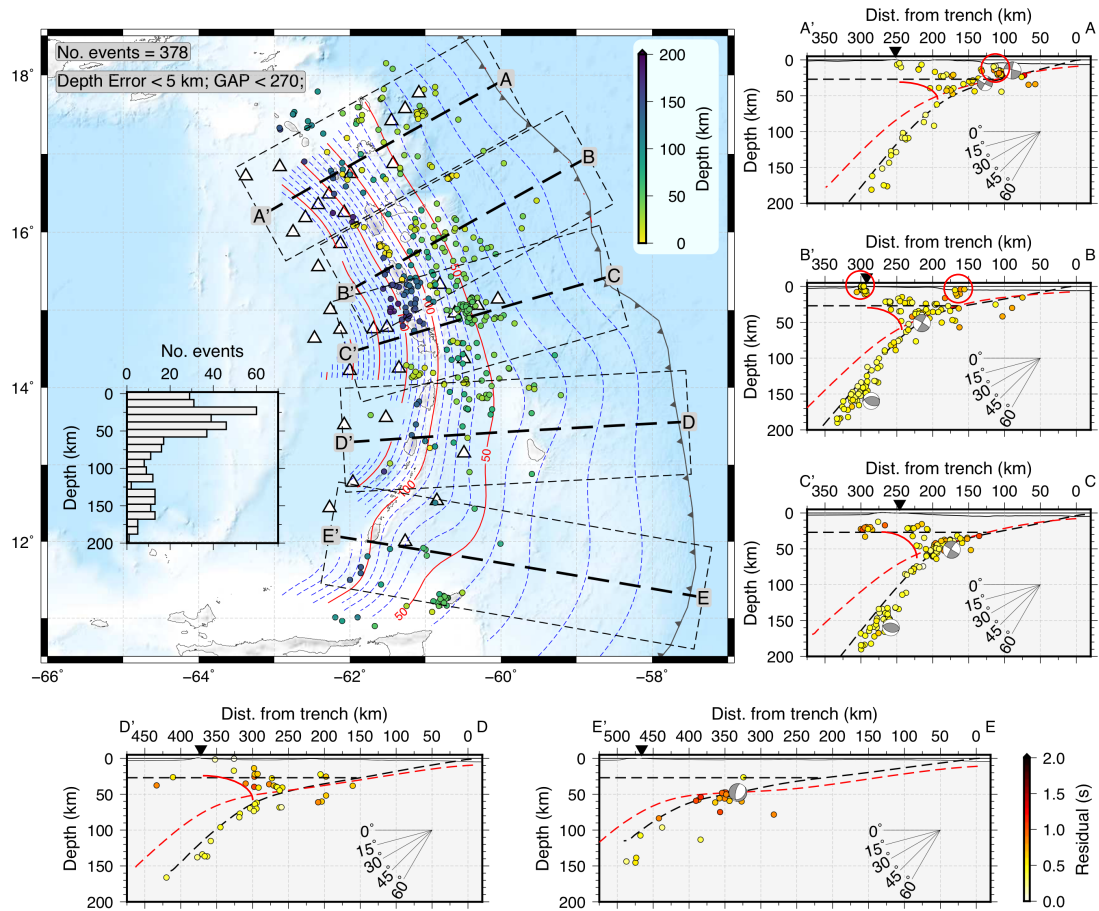


Figure 5. Distribution of the relocated 378 events coloured by hypocentral depth. The inset shows the number of events versus depth. Triangles are the stations from the VoiLA OBS deployment. Dashed blue and red lines represent the refined slab geometry from this study. Red curve delineates the wedge-shaped mantle corner seismicity. Depth profiles through the regional events comprise earthquakes that are within 75 km perpendicular distance of the labelled lines on the map. In the profiles, earthquakes are coloured by their RMS misfit after the relocation using the best 1-D velocity models from this study. The side hemisphere focal mechanisms from the Global Centroid Moment Tensor Project (see Data and Resources) are plotted. Black dashed curves are from slab model generated in this study, while the red dashed curves are from Slab2.0 (Hayes et al., 2018).

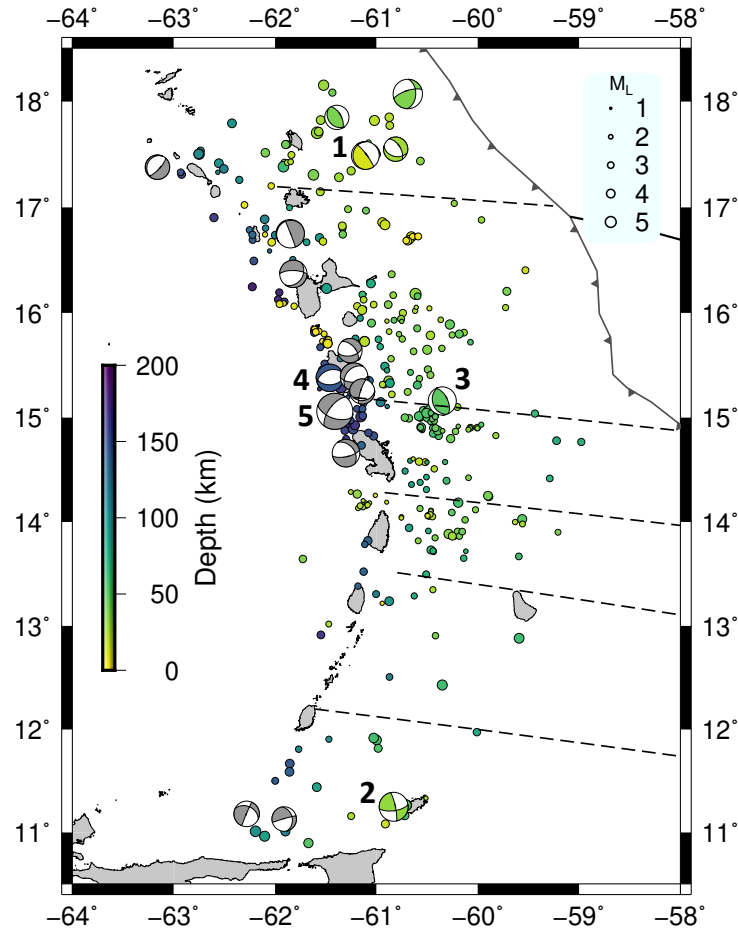


Figure 6. Local seismicity as derived from this study. Focal mechanisms (FM) for events with GCMT (see Data and Resources) solutions during the period of passive-seismic experiments are coloured by depth. Focal mechanisms for all historical deep (> 70 km) normal fault events (at least one slip direction between -145° and -90°) in the GCMT catalogue and from Gonzalez et al. (2017) are marked in grey. FM 1: M_w 5.7, 2017/04/17; FM 2: M_w 5.9, 2016/12/06; FM 3: M_w 5.8, 2017/02/03; FM 4: M_w 5.6, 2016/10/18; FM 5: M_w 7.4, 2007/11/29.